Ethane Oxidative Dehydrogenation with CO2 on thiogallates

Vera Bikbaeva, Olivier Pérez, Nikolay Nesterenko, Valentin Valtchev

ARTICLE

Ethane Oxidative Dehydrogenation with CO_2 on thiogallates

Vera Bikbaeva,[a] Olivier Perez, [b] Nikolay Nesterenko, [*c] and Valentin Valtchev[a]

Received 00th January 20xx,
Accepted 00th January 20xx

DOI: 10.1039/x0xx00000x

The CO_2-assisted oxidative dehydrogenation of ethane (ODH-CO_2) attracts a lot of research interest since it combines greenhouse gas utilization with the production of valuable chemicals. The present study demonstrates the potential of the novel non-classic catalysts, alkali thiogallates, in this reaction. The contribution also reports a novel solvothermal synthesis method to prepare crystalline $KGaS_2$ thiogallate materials. Despite the low surface area of the bulk $KGaS_2$ system, the material shows substantial activity in CO_2 to CO transformation with conversions in the range of 22-36% at 700-800 °C. The catalyst allows utilization of the co-produced hydrogen from ethane thermal cracking for CO_2 hydrogenation without substantially impacting ethylene yield even at 800°C at the conversion level of ethane close to 70%. The catalyst demonstrates stable performance with insignificant coke formation. The structure of the $KGaS_2$ thiogallate material is fully conserved after the reaction. These results open a promising opportunity for the thiogallate materials as catalysts with moderate hydrogenation function, which are highly tolerant to the CO and highly reactive hydrocarbons environments.

Introduction

Expansion in chemicals is one of the upcoming trends in the transformation of the petrochemical industry, and ethane transformation is an important part of the downstream evolution. A significant portion of the recent investments in olefins was in gas-based petrochemistry, either in ethane steam cracking (ethylene production) or in propane dehydrogenation (propylene production). The transition is a part of the efforts to transform "a fuel refinery" into the "refinery of the future".[1] However, the CO_2 emissions of a refinery of future per ton of olefins are significantly higher than traditional petrochemical production because the feedstock is produced on purpose via several hydrotreatment steps. Thus, an increase in the amount of chemicals production at a refinery from 10% to 25-40% may almost double the carbon footprint (CO_2/ton) from 1-1.5 to 2.4 -2.6.[2] Consequently, high carbon footprint is not acceptable given the zero-carbon emission target in the industry. In addition, the technologies to produce fossil products are less and less attractive for investors unless the production is low carbon. Thus, the downstream sector needs to rethink how olefins will be produced in the future. Among the options to decarbonize the production of chemicals, a combination of olefins production with CO_2 utilization is an important topic for the next decades in the quest for the downstream industry transformation. This approach may even lead to a carbon-negative technology for olefins production from the fossil feedstock.

The idea is to directly use the hydrogen produced as a by-product by the processes or benefit from the heat of the process with a low carbon/green H_2 co-feeding. This perspective requires the development of a new catalyst, which could selectively hydrogenate CO_2 in the presence of hydrocarbons. Metal sulfides are known for CO_2 hydrogenation to high-value products, such as methanol, dimethyl ether, CH_4, light alkenes, jet fuel, or CO. The MoS_2-based catalyst showed promising results in CO_2 methanation and methanol synthesis. For example, Hu et al.[3] investigated the CO_2 transformation over MoS_2 at 50 atm, 300 °C; this system resulted in MeOH with 94.3% selectivity. Primo et al.[4] applied oriented MoS_2 nanoplatelets at 10 atm at 300-600 °C for the CO_2 methanation with the 100% key product selectivity. ZnS was used for the direct non-oxidative dehydrogenation of ethane at 550 °C, showing only about 10% of conversion.[5] The thermal stability of this materials was not sufficiently at higher temperatures, where ethane conversion could reach more significant level. Thus, up to now, there is not any report on the utilization of metal sulfides for ODH-CO_2 of ethane.

Catalytic behavior of sulfur-free gallium-containing systems in ethane dehydrogenation and CO_2-assisted oxidative ethane dehydrogenation was also studied.[6,7] A significant influence of the nature of the substrate on the deactivation of Ga-containing catalysts in the ODH-CO_2 has been reported.[8] The samples exhibited low tolerance to coke formation. Most of the studies of ethane dehydrogenation on Ga-containing materials demonstrated the selectivity to ethene >90% with the low amount of the aromatic fraction[9]. Zeolites (HZSM-5,[6] HSSZ-13[9]) and oxides (TiO_2,[10] Al_2O_3[11,12]) were used as carriers of the Ga-containing active phase. However, for CO_2-assisted reactions on these catalytic systems, only the results at low conversion

[a] Laboratoire Catalyse et Spectrochimie, ENSICAEN, Université de Caen, CNRS, 6 Boulevard Maréchal Juin, 14050 Caen, France.
[b] Laboratoire de cristallographie et sciences des matériaux, ENSICAEN, Université de Caen, CNRS, 6 Boulevard du Marechal Juin, 14050 Caen, France.
[c] TotalEnergies One Tech Belgium, Zone Industrielle C, 7181 Seneffe, Belgium.

†Electronic Supplementary Information (ESI) available: including XRD and UV-vis data, SEM images, EDS analyses, and catalytic data. See DOI: 10.1039/x0xx00000x

were reported. The conversion was about 10% over Ga/TiO_2[10] at 700 °C, and only 3.2% over FeGa@ZSM-5[13] at 600 °C. The performance of unsupported Ga-containing materials is still seldom reported in the literature.

Alkali ternary thiogallates are one of the varieties of the unsupported Ga-containing materials. They exist in several structure types. The most known and the most well-studied is $AGaS_2$ (A=Na,[14] Cs,[15] Ag[16–18]) family of materials. Several novel members in this family, $Na_6Ga_2S_6$[19] and A_5GaS_4 (A=Li, Na), [20] were recently discovered.

A standard protocol for synthesizing the various ternary A_xGaS_y materials involves heating to 650-800 °C for several hours in the sealed quartz ampoule.[14,20] A few studies report the low-temperature synthesis route to alkali-containing ternary thiogallates, which is more advantageous for industrialization. For instance, $AgGaS_2$[18] was obtained at 300 °C under the N_2 atmosphere in the presence of oleates. The first solvothermal synthesis of $AgGaS_2$ was reported by J. Hu et al.[17] Tetragonal crystals (a = 5.7538 Å, c = 10.3026 Å) with the size of 5 – 12 nm were prepared using ethylenediamine as solvent and template at the same time at 180-230 °C for 10 h. Nanoflowers with similar composition ($AgGaS_2$) and the tetragonal unit cell (I-42d space group, a=5.76 Å and c=10.3 Å) were described by Yuan et al.[21] The nanocrystalline tetragonal phase (a = 5.523 Å, c = 11.141 Å) $CuGaS_2$ was also synthesized by a solvothermal approach by Lu et al.[22] In contrast, the literature is silent about a solvothermal crystallization of $AGaS_2$ (A=K, Na, Cs) in monoclinic configuration. Up to now, the monoclinic structure of $KGaS_2$,[23,24] $NaGaS_2$,[14] $CsGaS_2$ as well as $Cs_2Ga_2S_5$[25] were obtained only by solid-state reaction at 600-900 °C.

The alkali thiogallates, e.g., $AgGaS_2$, are known for their photocatalytic activities.[26,27] For instance, Lee and al. studied the photocatalytic activity of $AgGaS_2$ nanoparticles in H_2S splitting reaction to produce hydrogen.[26] The same group also reported the utilization of $AgGaS_2$-type photocatalyst for H_2 production from water.[28] Besides the photocatalytic activity, a distinctive feature of the alkali thiogallates is their exceptional thermal stability (800-900 °C) which is not very common for Ga-containing materials. Another advantage of these compounds is their potentially high coking resistance thanks to the sulfur present in the structure and their moderate hydrogenation activity. Hence, we considered these materials as potentially a promising catalytic system for the ethane ODH-CO_2 reaction.

For many metals, such as Mo and Fe, a transformation to the carbide phase occurs over 700 °C under a hydrocarbon environment.[29,30] In contrast, gallium carbide would not be formed under these conditions, which is also one more reason to focus on the alkali thiogallates. The alkali ternary thiogallates will remain in their initial state while preventing the reduction of gallium to the individual metal. These systems as catalysts for ethane oxidative dehydrogenation with CO_2 have never been reported.

The present study reports the synthesis of monoclinic potassium ternary thiogallate ($KGaS_2$) and its application in ODH-CO_2 of ethane.

Experimental

Catalyst preparation

The crystals of $KGaS_2$ were obtained via a solvothermal synthesis using Ga_2O_3 (99.99%, 50 mesh powder, Alfa Aesar), Sulfur (≥ 99.5%, Sigma-Aldrich), and KNO_3 (≥ 99.0%, Sigma-Aldrich) as reagents. Ethylenediamine (EDA) (≥ 99.5%, Fluka Analytical) and 1-2-(aminoethyl) piperazine (AEP) (98%, Alfa Aesar) were used as the solvent and the template, respectively. The solids were loaded in a molar ratio $Ga_2O_3/S/KNO_3$=1/25.5/2.3, followed by the addition of template (EDA or AEP) to the mixture. The resulting mixture was stirred at room temperature for 30 min. Then the suspension was transferred to a stainless-steel autoclave with Teflon liner and kept at 190 °C for 1-7 days under static conditions. The solid was recovered by filtration, washed with ethanol, and, eventually, dried at 50 °C for 1 h in an air atmosphere.

Material characterization

The powder X-ray diffraction (PXRD) analysis of the samples was performed with a PANalytical X'Pert Pro diffractometer using Cu Kα radiation (λ = 1.5418 Å).

Measurements of nitrogen sorption isotherms at -196 °C were carried out on Micromeritics ASAP 2020 surface area analyzer. The pretreated samples in nitrogen were analyzed after degassing at 300 °C. The microporous volume (V_{mic}, $cm^3 \cdot g^{-1}$) and the specific surface area (S_{ext}, $m^2 \cdot g^{-1}$) was obtained by the t-plot method. The crystal size and the morphology were studied by a field-emission scanning electron microscope (SEM, MIRA-LMH TESCAN) equipped with an energy-dispersive X-ray spectroscopy (EDS) analyzer. The EDS analyses were obtained with SDD detector.

Ultraviolet-visible (UV-Vis) spectra of the samples were recorded with Cary 4000 spectrometer from Varian. The spectrum acquisition was done between 800-200 nm with a speed of 300 nm/min.

Catalyst evaluation

300 mg of a catalyst (fraction 100–400 μm) was loaded to a fixed bed downflow quartz reactor. Prior to the reaction, all the catalysts were dried in the reactor at 350 °C under N_2 flow for 2 hours. Afterward, the catalyst was heated up from room temperature to the reaction temperature under the reactants flow with a 10 °C/min ramp rate. The test was terminated by stopping the flow of the reactants, switching to N_2 flow, and cooling down the set-up to the room temperature under N_2 flow.

The reaction effluent was analyzed online with a gas chromatograph (Interscience Compact GC) equipped with two TCDs and one FID. A molecular sieve 5A, Rt-QBond, Rtx-1 columns were used to separate light gases mixtures (H_2, N_2, CO, CO_2), light hydrocarbons mixture (CH_4, C_2H_4, C_2H_6) and aromatic hydrocarbons (from benzene till naphthalene), respectively. In all the experiments, N_2 was used as the internal standard to calculate the conversion and to closure the material balance.

The tests were performed with a $C_2H_6/CO_2/N_2$=/49.5/36.5/14 (vol.%) mixture (C_2H_6/CO_2 – 1/0.74 v/v) in the temperature

range 700-800 °C, at atmospheric pressure, WHSV (C_2H_6) = 5.9 h^{-1}.

The conversion and selectivities were obtained as follows:

$$Conversion(a) = \frac{C_{inlet}(a) - C_{outlet}(a)}{C_{inlet}(a)} \cdot 100\% \quad (1)$$

$$Carbon\ selectivity\ (i) = \frac{F(i)}{\sum F(i)} \cdot 100\% \quad (2)$$

$$where\ F(i) - mol\ \ of\ the\ C\ in\ the\ product\ compound$$

Results and discussion

Synthesis and characterization of the catalysts

In the presence of amines, the crystallization of gallium sulfides may occur in different pathways. The synthesis usually results in octahedral clusters, e.g., $Na_5(Ga_4S)(GaS_4)_3 \cdot 6H_2O$,[31] anionic layers, e.g. $[Ga_4S_7(en)_2]$[32] with gallium atoms trigonal-pyramidally coordinated by Sulfur, or $[GaS_2]^-$ layers, e.g., $NaGaS_2$.[14] In this contribution, we focused on a solvothermal synthesis of thiogallates with ethylenediamine and 1-2-(aminoethyl)piperazine. In the absence of the potassium cation, the preparation resulted in the amorphous phase with the AEP template and the non-defined low crystalline phase of gallium sulfide with the EDA template (Fig.S1). Representative SEM images of obtained solids are shown in Fig. S2. The presence of inorganic cations, e.g., potassium, plays the role of a structural directing agent and drives the formation of a well-crystallized material (Fig.S1). The resulted thiogallate, synthesized with potassium and EDA, was determined as $KGaS_2$.

The powder X-ray diffraction (PXRD) patterns of the obtained product powders showed patterns similar to $NaGaS_2$ and to $K_{0.56}Na_{0.44}GaS_2$.[14] The ICSD structure of $KGaS_2$ published in the Inorganic Crystal Structure Database (ICSD collection code 107928) refers to Delgado's study,[33] the object of which is the analysis of the compound $TlGaSe_2$. So, the assignment in the database was done for a compound of a different to $KGaS_2$ composition and remains questionable. To make a proper analysis of our PXRD patterns, the profile matching has been performed on the basis of two previously reported structural analysis of $KGaS_2$. A first structure solution of $KGaS_2$ using single crystal data resulted in the non-centrosymmetric space group Aa[34] (a=14.721(5) Å, b=10.425(3) Å, c=10.424(2) Å, ϒ=100.16 (2)°). By analogy with compounds $TlGaSe_2$ and $NaGaS_2$ compounds, a PXRD study proposes a new description in the centrosymmetric monoclinic space group C2/c (a=10.4136(2) Å, b=10.4143(2) Å, c=14.7866(2) Å, β = 100.165(2)°).[23] The result of the pattern matching analyses performed using Jana2006,[35] using these two references clearly indicates the purity and the quality of the different synthetized $KGaS_2$ samples (refined cell parameters: a=10.417(3) Å, b=10.399(3) Å, c=14.788(4) Å, β =100.129(3)°) (Fig. S3).

The synthesis of $KGaS_2$ with EDA crystals resulted in the crystals of 1-2 µm with a plate-like rectangular morphology (Fig.1a). The EDS analysis of the EDA-synthesized $KGaS_2$ crystals showed a uniform distribution of all the elements (Fig.2). According to the

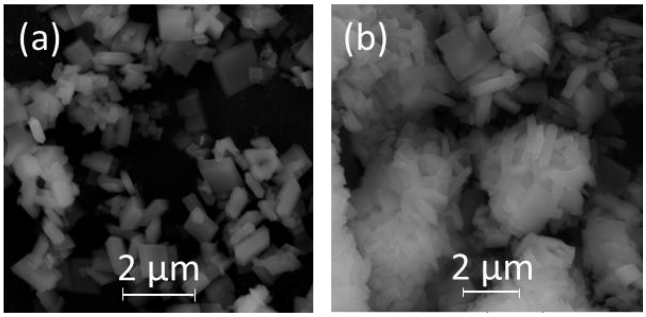

Fig.1 SEM images of $KGaS_2$ synthesized with EDA (a) and AEP (b).

EDS analysis, the molar ratio K: Ga: S was 1: 1: 1.9 (Fig.S4). The similar Ga/S ratio was reported in earlier studies for the alkali-containing thiogallates obtained by solid-state high-temperature synthesis.[14,36]

The collected UV-Vis spectra of $KGaS_2$ were identical to the $NaGaS_2$ spectra reported by V. Klepov et al.[14] (Fig. S5). The recorded spectrum showed a curve with the characteristic intense peak at 280 nm and the two weak peaks in the region of 330-470 nm. The specific surface area of the EDA-synthesized $KGaS_2$ determined by N_2 physisorption was 12 cm^2g^{-1}, which is a typical value for the non-porous material with a size of about 1 µm.

The physicochemical analysis of solvothermally synthesized K-thiogallates confirmed that they are structurally identical to the $KGaS_2$ obtained by solid-state high-temperature synthesis.

Synthesis optimization

The influence of the sulfur content on the crystallization results was studied. The products obtained with the molar ratio Ga/S/K=1/5.7/2.3, still showed the presence of some amorphous phase. At the same time, an excess of the sulfur in the mixture (molar ratio Ga/S/K=1/25.5/2.3) resulted in a solid of much higher crystallinity (Fig.3).

The crystallization time was varied from 1 to 7 days. After 1 day (Fig. S6), the product already contained a crystalline phase. The SEM analysis showed the presence of a mixture of crystallites of 200-300 nm and of 1-3 µm (Fig. S7). With further prolongation of the crystallization time to 4 days, the nanosized crystals disappeared, and the particle size distribution has become uniform. The changes in the crystal size were also coupled with an increase in X-ray crystallinity.

Further extension of the synthesis time to 7 days did not result in any further changes in morphology and crystallinity.

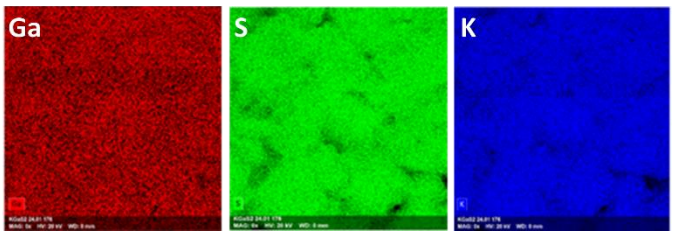

Fig.2 EDS elemental distribution in $KGaS_2$ (EDA, 4d, 190 °C).

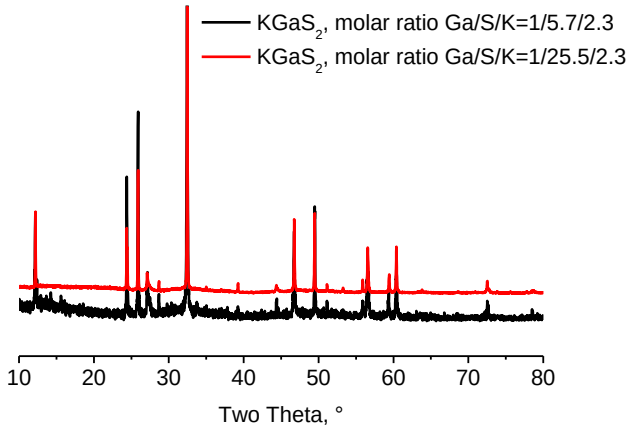

Fig.3 Powder XRD patterns of as-prepared $KGaS_2$ with two different Ga/S/K ratios (EDA, 7d, 190 °C).

The impact of ethanol and water on the formation of $KGaS_2$ was also investigated. Ethanol-water mixture was used as co-solvents in combination of the EDA template. The addition of ethanol led to a decrease in product crystallinity keeping the same crystallization time (Fig. S8 and S9). The SEM images revealed a significant presence of small nanoparticles with random morphology that are most probably amorphous (Fig.4). The obtained XRD patterns were similar to the simulated structure Shim et al [23](Fig. S9).

Catalytic performances

$KGaS_2$ thermal stability

At 600 °C, the measured conversion of thiogallate-based materials in CO_2 hydrogenation and ethane transformation was very limited, in the range of 1-2% of conversion. A noticeable increase in catalytic activity was observed with the temperature rise to 700 °C or higher. The most relevant range for, the ODH-CO_2 tests of ethane was found between 700-800 °C. Before using the novel material in high temperature reaction, it was necessary to confirm its thermal stability. In order to do so, a sample for $KGaS_2$ was subjected to 800 °C for 1 hour in N_2 flow, which was the highest temperature set point used in the catalytic experiments. The XRD analysis confirmed the retention of crystallinity (Fig. S10) and that the treatment did not result in morphological changes (Fig. S11).

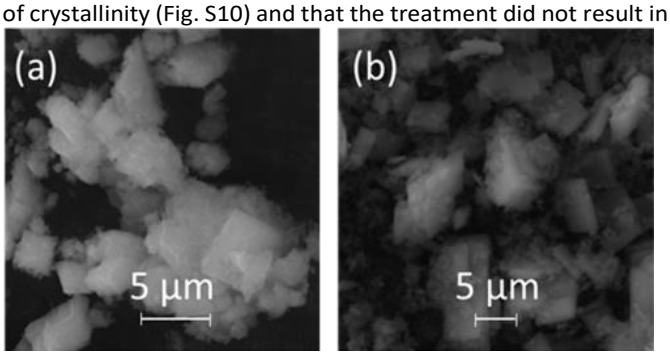

Fig.4 SEM micrographs of $KGaS_2$ prepared in (a) solvent system EDA-EtOH (2:1, volume ratio), and (b) EDA-EtOH-H_2O (2:1:1, volume ratio).

Blank test

In order to reveal the catalytic impact of the thiogallate-based materials on the reaction yield, a blank test without any catalyst was performed under the same operating conditions (same linear velocity, same temperature, same total and partial pressure of the reagents). In the blank test C2 (ethane), N_2, and CO_2 were co-fed in the same ratio as in the catalytic reaction ($C_2H_6/CO_2/N_2$=49.5/36.5/14 v/v/v). The blank test without ag catalyst is referred to in the text as a thermal process ("C2 thermal").

Performance in ODH-CO_2 of ethane

The presence of the thiogallate-based material in the reactor showed substantial difference in performances already at 700 °C (the lowest reaction temperature); the conversions of CO_2 increased from 2% to 22% (Fig. 5). Interestingly, the ethane conversion on thiogallate even exceeded the thermal value at 700 °C (Fig. 5). So, the material not only showed a substantial hydrogenation activity for CO_2, but also were able to hydrogenate CO_2 without destroying ethylene yield from ethane. The activity of the catalyst was stable for the tested time-on-stream of 225 min (Fig.S12).

However, upon further increase of the temperature to 750 °C, the thiogallate-based materials also started partially hydrogenate ethylene. The CO_2 conversion increased but the rise was relatively modest. Thus, due to the hydrogenation back of ethylene to ethane, the apparent ethane conversion decreased by 8% compared to the thermal one (Fig. 5).

Further temperature increases to 800 °C, resulted in a significant growth of both CO_2 and ethane conversions in the presence of the catalyst (Fig. 5). Although the catalyst still showed some ethylene hydrogenation, the difference with the thermal process decreased in comparison the one observed at 750 °C. In contrast, the CO_2 conversion reached the level of 36% at 800 °C, which was 12% higher relative to the one at 750 °C and roughly 13% lower than the thermodynamic equilibrium conversion (Fig. S13). The ethane conversion at 800 °C reached almost 70% what was relatively close to the thermodynamic value (Fig. S13).

Thus, the thiogallate-based material shows about 36% of CO_2 hydrogenation at 800 °C with only a minor impact on the ethylene yield and selectivity relatively to the thermal process (Fig.6).

One can also see that at 700 °C, the ODH-CO_2 of ethane on the thiogallate-based material results in the almost equivalent conversion of ethane and CO_2. That means that the produced hydrogen in ethane transformation to ethylene is almost fully utilized for CO_2 hydrogenating (Fig.5). In contrast, at 750 °C and 800 °C the conversion of CO_2 is roughly two times lower in comparison with the ethane conversion. This means that only half of the produced hydrogen was consumed for CO_2 hydrogenation.

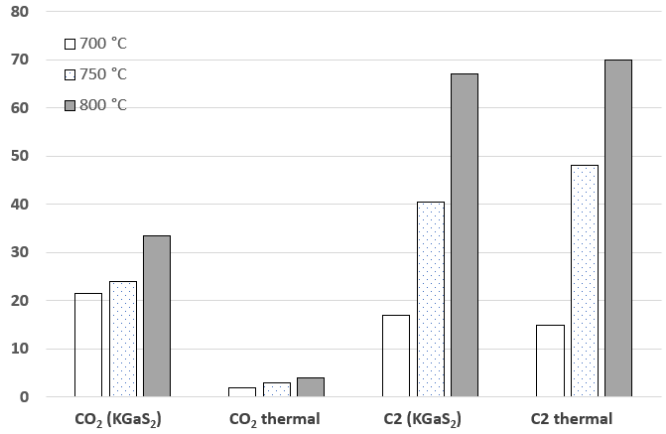

Fig.5 Comparison of C_2H_6 and CO_2 conversions on $KGaS_2$ -based catalysts with the thermal one (P = 1 atm, C_2H_6/CO_2 = 1/0.74, WHSV =5.9 h^{-1}).

One can see that the presented thiogallate-based materials have demonstrated a promising CO_2 hydrogenation activity that is comparable with the reported in literature for gallium oxide-based samples.[10,37]

The selectivity to the by-products (to heavies) on the alkali thiogallate catalyst is slightly higher than in the transformation without catalyst. The absolute values vary with the increase of the temperature due to a change in the predominant transformation pathways of ethylene but the impact on selectivity remains minor (Fig. 6).

Logically, the rise of the temperature from 700 to 800 °C resulted in higher methane production with the selectivity increase from 1 to 7%. However, the selectivities to methane remained comparable between the catalytic and the thermal processes.

One can see that the experimentally observed conversion level of ethane at 700 °C and 750 °C in both catalytic and non-catalytic tests remain at about 50% relative to the thermodynamic equilibrium conversion (Fig. S13). The latter shows only a limited impact of the catalyst on the ethane activation in the studied temperature range. The value

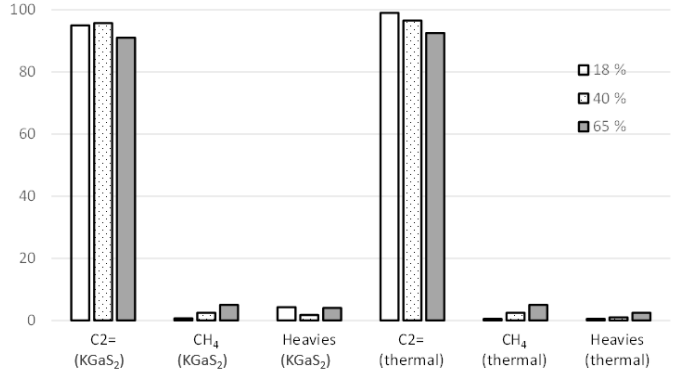

Fig. 6 Comparison of carbon molar selectivities on coke-free basis at the same conversion level of ethane (18%, 40%, 65%) for the thermal and the catalytic (over $KGaS_2$) routes (T =700-800 °C, P = 1 atm, C_2H_6/CO_2 = 1/0.74, WHSV =5.9 h^{-1}).

becomes much closer, almost reaching the thermodynamic level only at 800 °C.

In contrast, one can see that in the thermal non-catalytic process, the level of CO_2 conversion remains negligible, below 5% even at 800 °C. This value is more than order of magnitude lower relative to the equilibrium level of conversion. However, the introduction of the catalyst in the reactor allows achieving significantly higher conversion of CO_2, as high as 36 % at 800 °C. This value is not that far from the thermolytic equilibrium conversion of CO_2 of about 49% at 800 °C (Fig. S13). So, the catalyst clearly contributes to CO_2 activation and in the utilization of the formed hydrogen form the thermal ethane transformation for CO_2 transformation to CO.

Interestingly, an estimation of the thermodynamic equilibrium in the system containing CO_2 and ethane, H_2, CO, H_2O, and ethylene showed that the preferred reaction should be the dry reforming of CO_2 with ethane to CO and hydrogen with only a very limited selectivity to ethylene (Fig. S14). This reaction is undesirable for the ethylene synthesis from ethane and is not taking place without a specific catalyst. In contrast, the current $KGaS_2$ material preferentially catalyzes CO_2 hydrogenation in presence of ethylene with the hydrogen produced in-situ from the thermal conversion of ethane and substantially without making any significant production of heavy hydrocarbons and of methane.

The analysis of the spent catalysts after the reaction showed no formation of any amorphous or any other phases. The XRD pattern of the aged sample remained identical to the parent material before loading (Fig. 7). One can see no modifications of crystal morphology as well as no indications of any agglomerations or crystallites decompositions (Fig. 7).

Considering that the material was synthesized according to a new method and hasn't ever been tested before in high temperature applications, the observation is important and shows a perspective in further optimization of the catalytic performances of the alkali thiogallates-type materials.

Conclusions

Crystalline alkali thiogallates were synthesized under solvothermal conditions, which represents a novel alternative route to obtain these materials. The physicochemical properties, including the thermal stability, of thiogallates were studied and revealed that they are sufficiently stable to be used as high-temperature heterogeneous catalysts. The $KGaS_2$-based material showed promising performance in the ODH-CO_2 of ethane process in the temperature range of 700-800 °C. The process showed close to thermodynamic conversion of ethane at 800 °C with a significant utilization of the produced hydrogen for CO_2 transformation to CO. The conversion of CO_2 to CO was at the level of 22-36%. The catalyst showed insignificant coke formation and allowed obtaining similar levels of the ethane conversion as for the thermal decomposition substantially

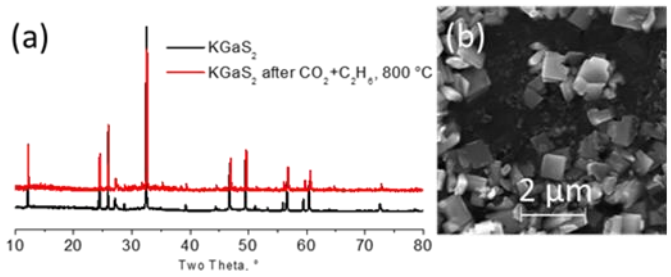

Fig.7 (a) PXRD patterns of as-prepared $KGaS_2$ and after ODH-CO_2 test (800 °C, P = 1 atm, C_2H_6/CO_2 = 1/0.74, WHSV =5.9 h^{-1}); (b) SEM images of $KGaS_2$ N_2-treated after ODH-CO_2 test (700 °C).

without making any additional production of by-products (heavy hydrocarbons, CH_4). The set of experimental results proves that the thiogallate catalysts could be of interest for the processes where a moderate hydrogenation function is required in the presence of CO and highly reactive hydrocarbons.

Author Contributions

Vera Bikbaeva: Investigation, methodology, and writing-original draft. Olivier Perez: Investigation. Nikolay Nesterenko: Conceptualization, supervision, writing-review and editing. Valentin Valtchev: Conceptualization, supervision, writing-review and editing.

Conflicts of interest

There are no conflicts to declare.

Acknowledgments

This research was supported by TotalEnergies, the Industrial Chair ANR-TOTAL "NanoClean Energy" (ANR-17-CHIN-0005-01), and project NanoCleanEnergy+ (Region Normandy).

Notes and references

1 Keith A. Couch, presented in part at the ME-TECH-2021, EPC MENA, virtual, February, 2021.
2 Br. Huovie, presented in part at the ME-TECH-2021, EPC MENA, virtual, February, 2021.
3 J. Hu, L. Yu, J. Deng, Y. Wang, K. Cheng, C. Ma, Q. Zhang, W. Wen, S. Yu, Y. Pan, J. Yang, H. Ma, F. Qi, Y. Wang, Y. Zheng, M. Chen, R. Huang, S. Zhang, Z. Zhao, J. Mao, X. Meng, Q. Ji, G. Hou, X. Han, X. Bao, Y. Wang and D. Deng, Sulfur vacancy-rich MoS_2 as a catalyst for the hydrogenation of CO_2 to methanol, *Nat. Catal.*, 2021, **4**, 242–250.
4 A. Primo, J. He, B. Jurca, B. Cojocaru, C. Bucur, V. I. Parvulescu and H. Garcia, CO_2 methanation catalyzed by oriented MoS_2 nanoplatelets supported on few layers graphene, *Appl. Catal. B Environ.*, 2019, **245**, 351–359.
5 F. Goodarzi, L. P. Hansen, S. Helveg, J. Mielby, T. T. M. Nguyen, F. Joensen and S. Kegnæs, The catalytic effects of sulfur in ethane dehydroaromatization, *Chem. Commun.*, 2020, **56**, 5378–5381.
6 Z. Shen, J. Liu, H. Xu, Y. Yue, W. Hua and W. Shen, Dehydrogenation of ethane to ethylene over a highly efficient Ga_2O_3/HZSM-5 catalyst in the presence of CO_2, *Appl. Catal. Gen.*, 2009, **356**, 148–153.
7 E. V. Lazareva, V. M. Bondareva, D. A. Svintsitskiy, A. V. Ishchenko, A. S. Marchuk, E. P. Kovalev and T. Yu. Kardash, Oxidative dehydrogenation of ethane over M1 MoVNbTeO catalysts modified by the addition of Nd, Mn, Ga or Ge, *Catal. Today*, 2021, **361**, 50–56.
8 E. Gomez, B. Yan, S. Kattel and J. G. Chen, Carbon dioxide reduction in tandem with light-alkane dehydrogenation, *Nat. Rev. Chem.*, 2019, **3**, 638–649.
9 Y. Cheng, H. Gong, C. Miao, W. Hua, Y. Yue and Z. Gao, Ga_2O_3/HSSZ-13 for dehydrogenation of ethane: Effect of pore geometry of support, *Catal. Commun.*, 2015, **71**, 42–45.
10 R. Koirala, R. Buechel, F. Krumeich, S. E. Pratsinis and A. Baiker, Oxidative Dehydrogenation of Ethane with CO_2 over Flame-Made Ga-Loaded TiO_2, *ACS Catal.*, 2015, **5**, 690–702.
11 S. P. Batchu, H.-L. Wang, W. Chen, W. Zheng, S. Caratzoulas, R. F. Lobo and D. G. Vlachos, Ethane Dehydrogenation on Single and Dual Centers of Ga-modified γ-Al_2O_3, *ACS Catal.*, 2021, **11**, 1380–1391.
12 W. Chen, M. Cohen, K. Yu, H.-L. Wang, W. Zheng and D. G. Vlachos, Experimental data-driven reaction network identification and uncertainty quantification of CO_2-assisted ethane dehydrogenation over Ga_2O_3/Al_2O_3, *Chem. Eng. Sci.*, 2021, **237**, 116534.
13 M. H. Jeong, K. S. Park, D. M. Shen, J. W. Moon and J. W. Bae, Dehydrogenation of ethane and subsequent activation of CO_2 on hierarchically-structured bimetallic FeM@ZSM-5 (M=Ce, Ga, and Sn), *Korean J. Chem. Eng.*, 2021, **38**, 1129–1138.
14 V. V. Klepov, A. A. Berseneva, K. A. Pace, V. Kocevski, M. Sun, P. Qiu, H. Wang, F. Chen, T. M. Besmann and H. Loye, $NaGaS_2$: An Elusive Layered Compound with Dynamic Water Absorption and Wide-Ranging Ion-Exchange Properties, *Angew. Chem. Int. Ed.*, 2020, **59**, 10836–10841.
15 D. Friedrich, M. Schlosser, R. Weihrich and A. Pfitzner, Polymorphism of $CsGaS_2$ – structural characterization of a new two-dimensional polymorph and study of the phase-transition kinetics, *Inorg. Chem. Front.*, 2017, **4**, 393–400.
16 J. Zhang, S. Zhu, B. Zhao, B. Chen and Z. He, A new method of synthesis on high-quality $AgGaS_2$ polycrystalline, *Curr. Appl. Phys.*, 2010, **10**, 544–547.
17 J. Hu, Q. Lu, K. Tang, Y. Qian, J. Hu, Q. Lu, K. Tang, Y. Qian, G. Zhou and X. Liu, Solvothermal reaction route to nanocrystalline semiconductors $AgMS_2$ (M=Ga, In), *Chem. Commun.*, 1999, 1093–1094.
18 H. Wu, X. Li, Y. Cheng, Y. Xiao, Q. Wu, H. Lin, J. Xu and Y. Wang, The synergistic role of double vacancies within $AgGaS_2$ nanocrystals in carrier separation and transfer for efficient photocatalytic hydrogen evolution, *Catal. Sci. Technol.*, 2019, **9**, 5838–5844.
19 B. Eisenmann and A. Hofmann, Crystal structure of hexasodium di-µ-thiobis(dithiogallate) — II, $Na_6Ga_2S_6$, *Z. Für Krist. - Cryst. Mater.*, 1991, **197**, 143–144.
20 S. Balijapelly, P. Sandineni, A. Adhikary, N. N. Gerasimchuk, A. V. Chernatynskiy and A. Choudhury, Ternary alkali ion thiogallates, A_5GaS_4 (A = Li and Na), with isolated tetrahedral building units and their ionic conductivities, *Dalton Trans.*, 2021, **50**, 7372–7379.
21 Y. Yuan, J. Zai, Y. Su and X. Qian, Controlled synthesis of monodispersed $AgGaS_2$ 3D nanoflowers and the shape evolution

from nanoflowers to colloids, *J. Solid State Chem.*, 2011, **184**, 1227–1235.
22 Q. Lu, J. Hu, K. Tang, Y. Qian, G. Zhou and X. Liu, Synthesis of Nanocrystalline $CuMS_2$ (M = In or Ga) through a Solvothermal Process, *Inorg. Chem.*, 2000, **39**, 1606–1607.
23 S. Shim, W. B. Park, M. Kim, J. Lee, S. P. Singh and K.-S. Sohn, Cyan-Light-Emitting Chalcogenometallate Phosphor, $KGaS_2:Eu^{2+}$, for Phosphor-Converted White Light-Emitting Diodes, *Inorg. Chem.*, 2021, **60**, 6047–6056.
24 D. Friedrich, M. Schlosser, M. Etter and A. Pfitzner, Influence of Alkali Metal Substitution on the Phase Transition Behavior of $CsGaQ_2$ (Q = S, Se), *Crystals*, 2017, **7**, 379.
25 D. Friedrich, F. Pielnhofer, M. Schlosser, R. Weihrich and A. Pfitzner, Synthesis, Structural Characterization, and Physical Properties of $Cs_2Ga_2S_5$, and Redetermination of the Crystal Structure of Cs_2S_6, *Chem. - Eur. J.*, 2015, **21**, 1811–1817.
26 J. S. Jang, S. H. Choi, N. Shin, C. Yu and J. S. Lee, *J. Solid State Chem.*, 2007, **180**, 1110–1118.
27 K. Yamato, A. Iwase and A. Kudo, $AgGaS_2$-type photocatalysts for hydrogen production under visible light: Effects of post-synthetic H_2S treatment, *ChemSusChem*, 2015, **8**, 2902–2906.
28 S. H. Choi, J. S. Jang, N. Shin and J. S. Lee, Characterization of $AgGaS_2$-type Photocatalysts for Hydrogen Production from Water Under Visible Light, in *AIP Conference Proceedings*, AIP, Stanford, California (USA), 2007, **882**, 628–630.
29 Z. Zhao, F. Qin, S. Kasiraju, L. Xie, Md K. Alam, S. Chen, D. Wang, Z. Ren, Z. Wang, L. C. Grabow and J. Bao, Vertically Aligned MoS_2/Mo_2C hybrid Nanosheets Grown on Carbon Paper for Efficient Electrocatalytic Hydrogen Evolution, *ACS Catal.*, 2017, **7**, 7312-7318.
30 Y. Luo, L. Tang, U. Khan, Q. Yu, H.-M. Cheng, X. Zou and B. Liu, Morphology and surface chemistry engineering toward pH-universal catalysts for hydrogen evolution at high current density, *Nat. Commun.*, 2019, **10**, 269.
31 J. Rumble and P. Vaqueiro, $Na_5(Ga_4S)(GaS_4)_3{\cdot}6H_2O$: A three-dimensional thiogallate containing a novel octahedral building block, *Solid State Sci.*, 2011, **13**, 1137–1142.
32 P. Vaqueiro, From One-Dimensional Chains to Three-Dimensional Networks: Solvothermal Synthesis of Thiogallates in Ethylenediamine, *Inorg. Chem.*, 2006, **45**, 4150–4156.
33 G. E. Delgado, A. J. Mora, F. V. Pérez and J. González, Growth and crystal structure of the layered compound $TlGaSe_2$, *Cryst. Res. Technol.*, 2007, **42**, 663–666.
34 P. Lemoine, D. Carré and M. Guittard, Structure du sulfure de gallium et de potassium, $KGaS_2$, *Acta Crystallogr. C*, 1984, **40**, 910–912.
35 V. Petříček, M. Dušek and L. Palatinus, Crystallographic Computing System JANA2006: General features, *Z. Für Krist. - Cryst. Mater.*, 2014, **229**, 345–352.
36 S. Paderick, M. Kessler, T. J. Hurlburt and S. M. Hughes, Synthesis and characterization of $AgGaS_2$ nanoparticles: a study of growth and fluorescence, *Chem. Commun.*, 2017, **54**, 62–65.
37 B. Zhao, Y. Pan and C. Liu, The promotion effect of CeO_2 on CO_2 adsorption and hydrogenation over Ga_2O_3, *Catal. Today*, 2012, **194**, 60–64.